Vietnam Journal of Science and Technology ***58*** *(4) (2020) 461-472*

doi:10.15625/2525-2518/58/4/14702

EFFECTS OF WELDING CURRENT ON THE SHAPE AND MICROSTRUCTURE EVOLUTION OF THIN-WALLED LOW-CARBON PARTS BUILT BY WIRE ARC ADDITIVE MANUFACTURING

Le Van Thao[1, *], Hoang Quang Huy[3], Tran Van Chau[1], Mai Dinh Si[1], Dinh Duc Manh[1], Doan Tat Khoa[2]

[1]*Advanced Technology Centre, Le Quy Don Technical University, 236 Hoang Quoc Viet, Bac Tu Liem, Ha Noi, Viet Nam*

[2]*Mechanical Engineering Department, Le Quy Don Technical University, 236 Hoang Quoc Viet, Bac Tu Liem, Ha Noi, Viet Nam*

[3]*Weapon Institute, 51 Phu Dien, Bac Tu Liem, Ha Noi, Viet Nam*

[*]Email: *thaomta@gmail.com*

Received: 17 December 2019; Accepted for publication: 30 June 2020

Abstract. Wire arc additive manufacturing (WAAM) is nowadays gaining much attention from both the academic and industrial sectors for the manufacture of medium and large dimension metal parts because of its high deposition rate and low costs of equipment investment. In the literature, WAAM has been extensively investigated in terms of the shape and dimension accuracy of built parts. However, limited research has focused on the effects of welding parameters on the microstructure characteristics of parts manufactured by this process. In this paper, the effects of the welding current in the WAAM process on the shape and the microstructure evolution of thin-walled low-carbon steel components were studied. For this purpose, the thin-walled low-carbon steel samples were built layer-by-layer on the substrates by using an industrial gas metal arc welding robot with different levels of the welding current. The shape, microstructures, and mechanical properties of the thin-walled samples were then analyzed. The obtained results show that the welding current plays an important role in the shape stability, but it insignificantly influences the microstructure evolution of thin-walled samples. The increase in the welding current only leads to a coarser grain size and decreases the hardness of each zone of the walls. The mechanical properties (i.e. hardness and tensile properties) of the WAAM thin-walled low-carbon steel parts are also comparable to those of wrought low-carbon steel, and to be adequate with real applications.

Keywords: wire arc additive manufacturing, low-carbon steel, microstructures, mechanical properties.

Classification numbers: 2.9.1, 5.1.1, 5.1.4.

1. INTRODUCTION

In the last three decades, additive manufacturing (AM) is one of the hot topics in the manufacturing and engineering fields thanks to its capability of building complex components by adding materials layer-by-layer [1]. Among metal-based AM technologies, wire arc additive manufacturing (WAAM), which uses an electric arc as the heat source and a solid wire as the feedstock material, reveals as a prospective technique for manufacturing metal parts with medium to large size and medium geometric complexity. This technique presents a high material deposition rate up to 10 kg/h and lower costs of equipment investment [2]. In the WAAM processes, the arc is established between the tip of consumable wire and the workpiece under the protection of a shielding gas [3–5]. The arc heat source of WAAM processes can be gas metal arc welding (GMAW), gas tungsten arc welding (GTAW), and plasma arc welding (PAW). In terms of the productivity, the deposition rate of GMAW-based AM is two or three times higher than those of GTAW-based and PAW-based AM processes [6]. Hence, the GMAW-based AM process is more suited for the manufacture of parts with large dimensions.

In the literature, many studies have investigated the effects of WAAM process parameters on the shape of built components. For example, Zhang *et al*. [6] studied the effects of process parameters on the width and height dimensions of thin-walled components manufactured by low pulsed laser-assisted MIG arc welding. Xiong *et al*. [7] investigated the influence of main process parameters such as inter-layer temperature, wire feed speed and travel speed on the surface roughness. They demonstrated that the increase of travel speed could enhance the surface quality. Xiong and Zhang [8] developed a sensing and control system to keep the top surface distance of the GMAW-based AM-built thin-walled component constant.

In terms of the effect of the WAAM process on the internal quality of built materials, Suryakumar *et al*. [9] highlighted that thermal cycles did not have significant effects on material properties after five layers when building a thin-walled component. Liberini *et al*. [10] studied the effects of the voltage and the travel speed on the microstructures and hardness of GMAW-based AM-built thin-walled components. However, the tensile properties of the GMAW-based AM-built samples were not investigated yet. Chen *et al*. [11] also investigated the microstructure and mechanical characteristics of stainless steel 316L manufactured by the GMAW-based AM process. The authors reported that the tensile property of GMAW-based AM-built 316L steel were comparable to those of wrought 316L.

In Viet Nam, the research on metal-based AM and WAAM technologies is still very limited. This is because the metal-based AM systems are very expensive and they are not available yet in Vietnamese institutes and universities. Recently, some Vietnamese research teams have paid their attention on metallic AM technologies. Nguyen *et al*. [12] studied the microstructure and other properties of Ti6Al4V samples produced by selective laser sintering (SLS) technology. Le *et al*. [13] used an industrial GMAW robot to build successfully thin-walled 308L steel components according to the WAAM process. The authors also stated that the mechanical properties of WAAM 308L walls were comparable to those of wrought 308L steel.

In this study, the effects of the welding current on the shape stability and the microstructures of WAAM thin-walled low-carbon steel parts were investigated. For this purpose, the thin-walled samples were built on the substrates by using an industrial GMAW robot with different levels of welding current (Section 2). Thereafter, the effects of the welding current on the shape, the microstructure evolution and mechanical properties of built thin-walled samples were analyzed and discussed in Section 3. Section 4 summarizes some findings of this study.

2. MATERIALS AND METHODS

2.1. Materials

The GMAW-based AM system used in this study is shown in Figure 1a. This system uses an industrial 6-axis robot Panasonic TA-1400 (1) to execute the movement of the welding torch (4) during the deposition of materials on the substrates (Figure 1b). The motions of the robot are controlled by the robot controller (2), whereas the welding process parameters are controlled by the welding power source (3).

In this work, two low-carbon steel plates (SS400) with dimensions of 250 mm in length, 100 mm in width, and 10 mm in thickness were used to build the test samples. A commercial copper-coated low-carbon steel welding wire (ER70S-6) with a diameter of 1.2 mm was used to build the thin walls on the substrates. The chemical compositions of the welding wire and the substrate metal are shown in Table 1.

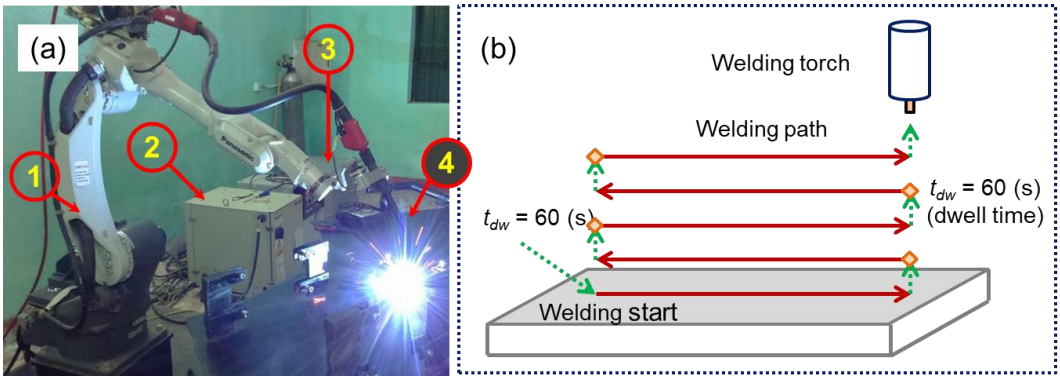

Figure 1. The GMAW-based AM system (a) and the strategy for building thin-walled samples (b).

Table 1. Chemical compositions of wire and substrate materials (in wt. %).

Element	C	Si	Mn	P	S	Al	Ca	Cu	Fe
Wire (ER76S-6)	0.04	0.92	0.45	0.011	0.015	-	-	0.2	Balance
Substrate (SS400)	0.05	0.037	0.46	0.013	0.002	0.044	0.0017	-	Balance

2.2. Experimental methods

Figure 1b shows the strategy for manufacturing thin-walled samples. The distance between the GMAW torch and the workpiece is 12 mm. When a welding layer is finished, the welding torch retracts to the beginning point of the next layer with a dwell time of 60 s. The dwell time between two adjacent layers was applied to cool down the workpiece and transfer the accumulated heat to the environment. In the experiments, no preheating was applied to the substrate, and the deposition was performed at room temperature. During the building process, a gas of 99.99 % CO_2 with a constant flow rate of 18 L/min was used for the shielding. The final cooling was carried in calm air at room temperature.

In the first experiment, four thin-walled samples (Figure 2a) were built on a substrate by using different levels of the welding current, as given in Table 2. The welding current was varied from 50 A to 110 A with an increment of 20 A, while the voltage and the travel speed of the welding torch were kept constant: the voltage is equal to 17.5 V, and the travel speed of the welding torch equals 300 mm/min. The dimensions of each built thin wall are approximately 80 mm in length, 16 mm in height, and from 3.34 mm to 4.86 mm in width.

Table 2. Process parameters of the welding process for building thin-walled samples.

Parameter / Sample	Welding current (A)	Voltage (V)	Travel speed (mm/min)
Sample 1	50	17.5	300
Sample 2	70	17.5	300
Sample 3	90	17.5	300
Sample 4	110	17.5	300

To observe the microstructures and measure the hardness of built materials, a specimen (Figure 2b) was cut off from the thin-walled samples and the substrate in the middle region (Figure 2a) by using a wire-cut electrical discharge machining (EDM) machine. The EDM-cut surface of this specimen was then grinded and chemically etched (Figure 2b) to ensure the analyzed material is well extracted from the built thin-walled samples. The microstructures of four built samples were observed by using an optical microscope of Carl Zeiss Company (AXIO A2M). The hardness of built materials was measured by a digital microhardness tester (Future-Tech Vicker FV-310) with a load of 5 kgf (49.05 N). The microstructure observation and hardness measurement results were presented in Section 3.2 and 3.3, respectively.

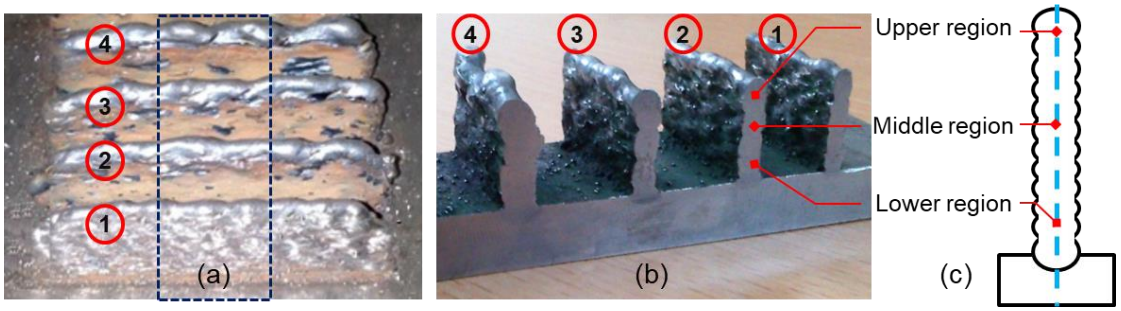

Figure 2. (a) Four thin-walled samples built on the substrate, (b) the EDM-cut specimen, and (c) three zones to observe the microstructures and measure the hardness of built materials.

The tests for observing the tensile properties of built thin-walled materials were carried out after examining the influence of the welding current on the shape and the microstructure evolution of the built thin-walled samples. The tensile tests were conducted on a tensile test machine of INSTRON Company (INSTRON 3369). The preparation of tensile test specimens and results were presented in Section 3.4.

3. RESULTS AND DISCUSSION

3.1. Macro observation

As shown in Figure 2, it is firstly found that the thin-walled samples built with lower welding currents (sample 1 and sample 2) reveal a shape more stable than that of the samples built with higher levels of the welding current (sample 3 and sample 4). In fact, when increasing the welding current, the heat input increases too [14]. As a result, the cooling time of the whole thin-walled part increases [15]. Moreover, due to an excessive heat input, the molten metal was subsided at a certain height of the thin wall, and the built walls show more distortion, e.g. the samples 3 and 4 in Figure 2b. On the other hand, the reduction in the welding current results in the decrease in the heat input [14]. This leads to a decrease in the solidification time. Thus, the thin walls built with a lower level of welding current reveal more stable shape. Moreover, the width of the walls built with lower welding current is smaller than that of the walls built with higher welding current [16]. The width of the walls 1, 2, 3, and 4 are 3.34 ± 0.10 (mm), 3.73 ± 0.12 (mm), 3.98 ± 0.18 (mm), and 4.86 ± 0.13 (mm), respectively. This is because the welding current in the GMAW process is in nearly linear relation with the wire feed speed. An increase in the welding current leads to an increase in the quantity of deposited materials. Based on this observation, it can be concluded that the welding current is one of factors that significantly influence the shape of built thin walls.

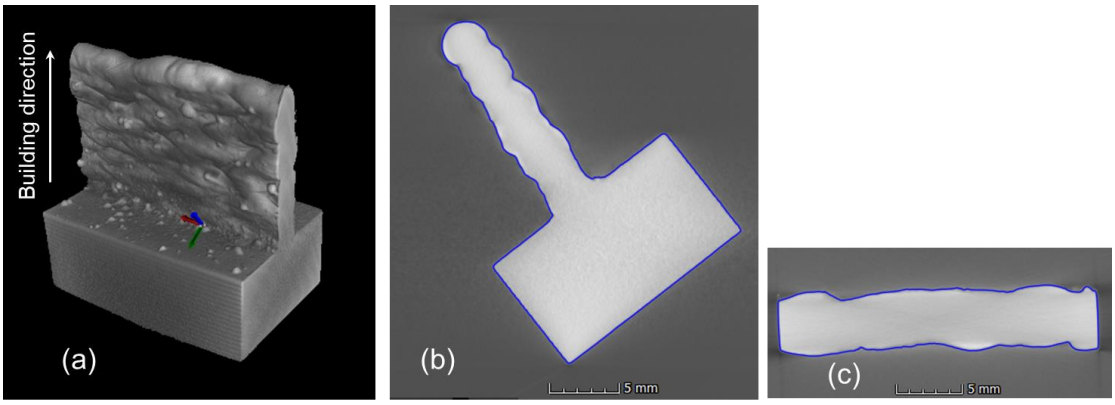

Figure 3. (a) Data obtained by the X-ray CT scan method for the sample 2, (b) a cross-section in the plane parallel to the building direction of the wall, and (c) a cross-section in the plane perpendicular to the building direction of the wall.

Lastly, from the data obtained by using X-ray CT scan method of all thin-walled samples (e.g. Figure 3 for the thin-walled sample 2), all built thin-walled samples do not show any major defects (e.g. cracks and pores) in both the welded metal and the interface zones between the deposited material and the substrate. This observation confirms that the consumable wire is a suitable material for additive manufacturing.

3.2. Microstructure observation

Based on the microstructure images obtained by the AXIO A2M optical microscope, it is found that all thin-walled samples 1, 2, 3 and 4 reveal the same microstructure evolution. They present similar microstructure types in each region of the built thin walls: the upper region, the middle region, and the lower region (Figure 2c). However, the welding current has the effect on the grain size of the built samples, particularly in the middle and lower regions. The samples built with higher welding current reveal coarser grains. In fact, an increase in the welding current leads to an augmentation in the heat input [14]. With higher heat input used, the solidification

time and the cooling time increase. Thus, the grain size becomes coarser. Figure 4 shows a comparison in terms of grain size between the sample 1, which was built with the lowest welding current and the sample 4, which was built with the highest welding current.

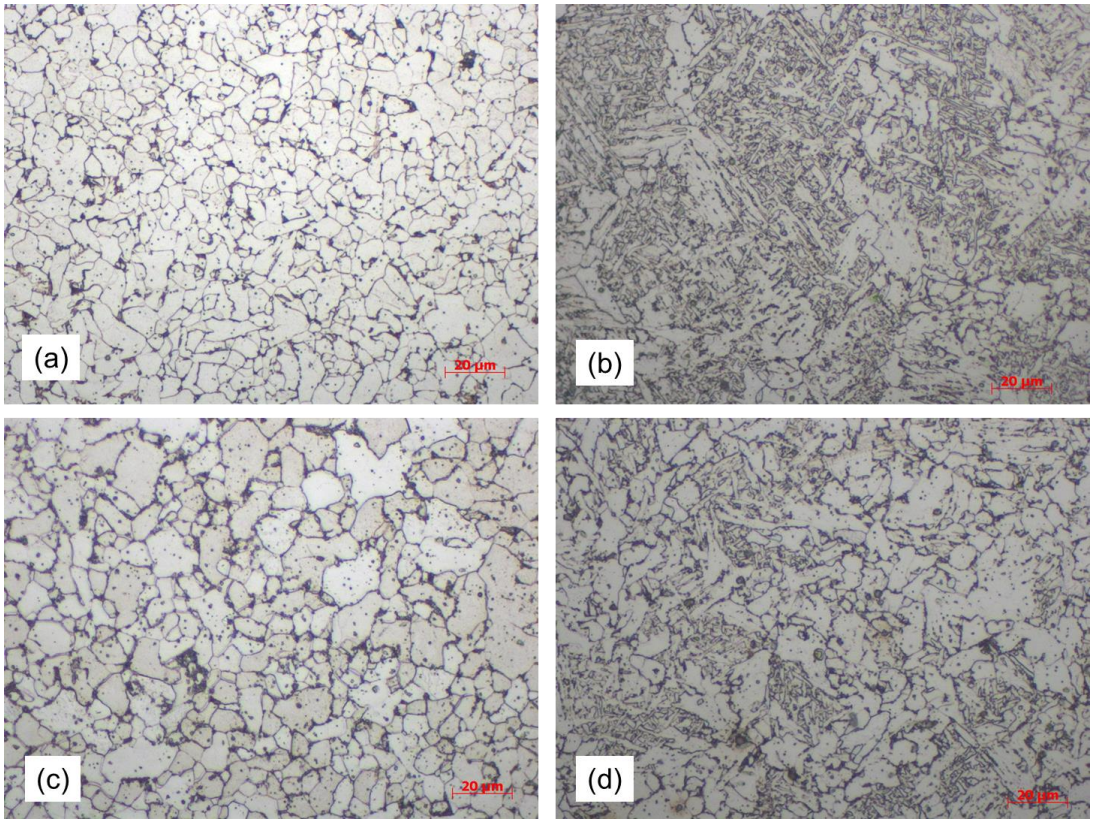

Figure 4. Microstructure in high magnification (500x) of the sample 1 in the middle region (a) and in the lower region (b), and those of the sample 4 in the middle region (c) and in the lower region (d).

As revealed in Figure 4, in the middle region, the microstructure of the sample 4 (Figure 4c) is coarser than that of the sample 1 (Figure 4a). The average grain size in the middle region of the sample 4 (Figure 4c) is about 13.3 (μm), which is higher than that of the sample 1 (Figure 4a), about 11.2 (μm). Due to the mix of equiaxed and lamellar structures in the lower region of the built walls (e.g. Figure 4b and 4d), it is difficult to quantitatively evaluate the grain size in this region. However, it can be observed that the microstructure in the lower region of the sample 1 (Figure 4b) exhibits more lamellar structures than those of the sample 4 (Figure 4d).

3.2.1 Microstructures in the upper region

Figure 5a shows the microstructure in the upper region of the built thin wall, which reveals lamellar structures composed of ferrites with different types of grains: allotriomorphic ferrite α, Widmanstätten ferrite α_w, and acicular ferrite α_a. This microstructure type is due to the combined influence of continued air cooling and heat conduction from the upper to the bottom region of the built samples. Moreover, the upper region (i.e. the last deposited layer) contacts the calm air at room temperature and it is not reheated and partially remelted by the heat that forms another

layer as in the middle region. Thereby, the primary austenite dendrite was transformed into typical Widmanstätten ferrites α_w.

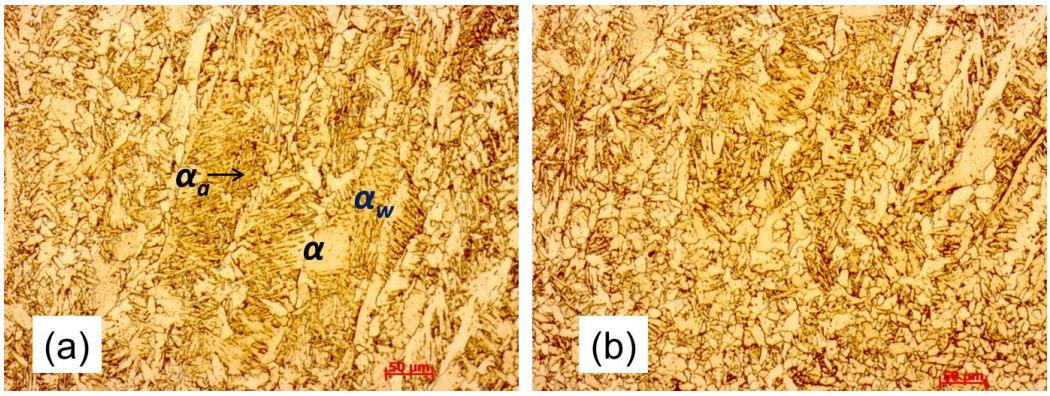

Figure 5. Microstructures in magnification 100x of the upper region (a) and the transition of microstructures between the upper and middle regions (b).

It is also found a transition of microstructures between the upper and middle regions. The mixed microstructures consist of lamellar microstructures of the upper region and equiaxed microstructures of the middle region (Figure 5b).

3.2.2. Microstructures of the middle region

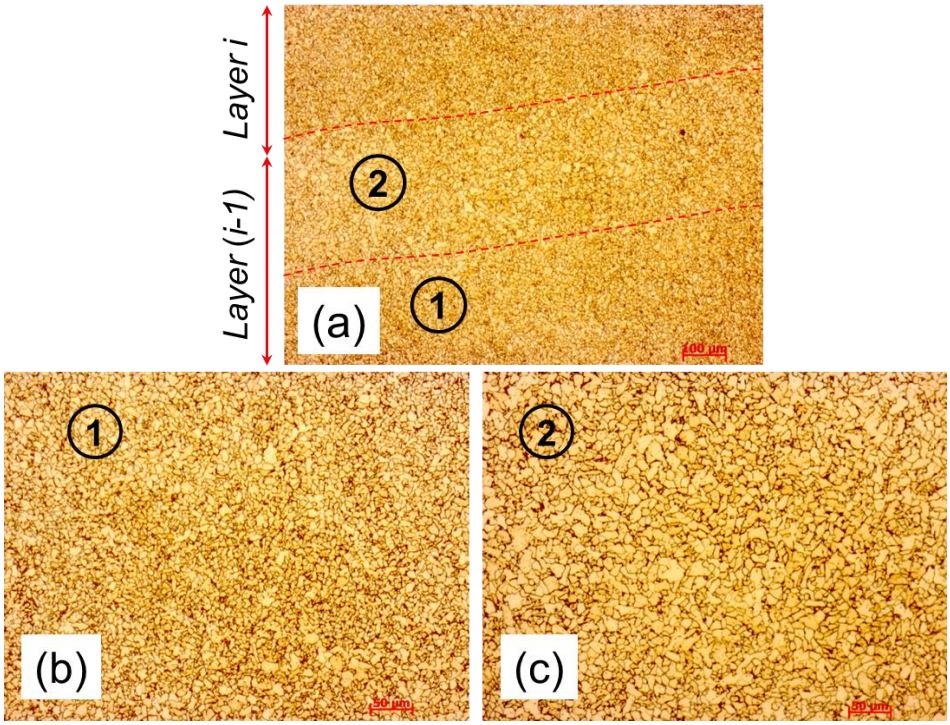

Figure 6. Microstructures in low magnification 50x of thin-walled part in the middle region revealed as granular structures (a), the microstructures in higher magnification 100x in the center of a layer (b), and in the overlapped zone (c).

The middle region is mainly characterized by granular structures of ferrite with small regions of pearlite at grain boundaries (Figure 6 and Figures 4a, 4c). All layers in the middle region reveal the same microstructure type. Moreover, the microstructures of this region could be classified into two types: granular grains in the overlapped zone (2) with larger sizes between two successive layers (Figure 6c) and equiaxed grains with relatively smaller sizes and denser distribution in the center of a layer (1) (Figure 6b). Due to the heat of molten pool, which forms the current deposited layer (*i*), the last built layer (*i*-1) was reheated and partially re-melted, resulting in coarser grains in the overlapped zone.

3.2.3. Microstructures of the lower region

The microstructures in the lower region consist of equiaxed grains of ferrite, in which thin lamellae are dispersed. The ferrite coexists in equiaxed form with thin strips of pearlite (Figures 4b and 4d). The grain size of the lower region is also finer than that of the middle region. The reason is that the lower region (including several first deposited layers) contacts the substrate at room temperature, while the middle zone contacts warm deposited layers [10]. Hence, the cooling rate in the lower region is higher than other regions. In addition, the middle zone presents the thermal gradient lower than that of the lower zone [15].

In summary, the welding current does not have significant effects on the microstructure evolution of built thin walls. All thin-walled samples show the same microstructure type in each region: lamellar structures in the upper region, granular structures of ferrites with small amount of pearlites at grain boundaries in the middle region, and the mix of equiaxed and lamellar structures in the lower region. The microstructure variation of the built sample is mainly due to the reheating and re-melting effect of depositing successive layers and the cooling condition.

3.3. Hardness

The hardness of built materials was measured in three regions of the built thin-walled samples: the upper region, the middle region, and the lower region (Figure 2c). For each sample, the hardness was measured at five locations in each region. These locations were selected approximately on the centerline of the cross section from the top to the bottom of the sample. The distance between two successive measured locations in each region is 0.5 mm. From the top of the samples, the measured locations distribute from 1 mm to 3 mm for the upper region, from 7 mm to 9 mm for the middle region, and from 13 mm to 15 mm for the lower region. The hardness value at each measured location plotted in Figure 7 on the left is the average value of three different indentations on the polished surface of the samples.

It is found that all the built samples reveal the same hardness evolution (Figure 7). For all samples, the upper region presents the highest hardness value and the middle region has the lowest hardness value. For example, in the case of the sample 1 (I = 50 A), the average hardness values are 192 ± 4.30 (HV) in the upper region, 162.4 ± 2.88 (HV) in the middle region, and 176.6 ± 4.56 (HV) in the lower region. This observation is coherent with the microstructure observed in Section 3.2. Due to the presence of Widmanstätten structures (Figure 5), the hardness of the upper region is higher than that of other regions. Because of the presence of lamellae structures, the lower region (e.g. Figure 4b and 4d) has the hardness values higher than that of the middle region, which dominantly consists of equiaxed structures (e.g. Figure 4a and 4c).

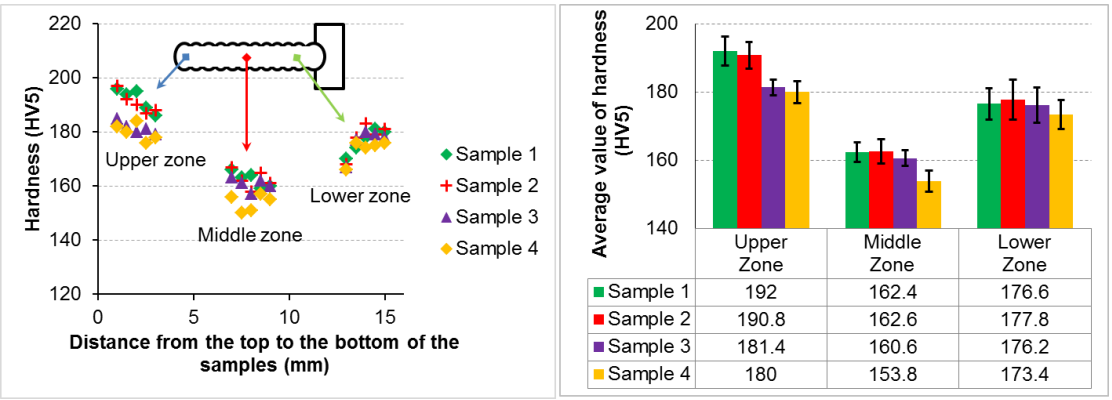

Figure 7. On the left: hardness measurement in the upper zone, the middle zone, and the lower zone of four samples, and on the right: the average value and standard deviation of hardness in each zone.

Moreover, when the welding current increased from 70 A to 110 A, the hardness of the built samples in each region was reduced (Figure 7 on the right). There is no significant difference on average hardness values in each region between the sample 1 (I = 50 A) and the sample 2 (I = 70 A). The sample 4 built with the highest welding current (i.e. with the highest heat input) is softer than other samples. In three regions, this sample reveals the lowest average values: 180 ± 3.16 (HV) in the upper region, 153.8 ± 3.11 (HV) in the middle region and 173.4 ± 4.22 (HV) in the lower region.

Lastly, the average hardness value in the upper and lower regions of all built thin-walled samples are higher than the maximum hardness value (168 HV) of wrought ASTM A36 low-carbon steel, which has nearly identical chemical composition regarding with ER70S-6 [17]. On the other hand, the average hardness value in the middle region of all samples is relatively lower than the maximum hardness value (168 HV) of wrought ASTM A36 steel.

3.4. Tensile property

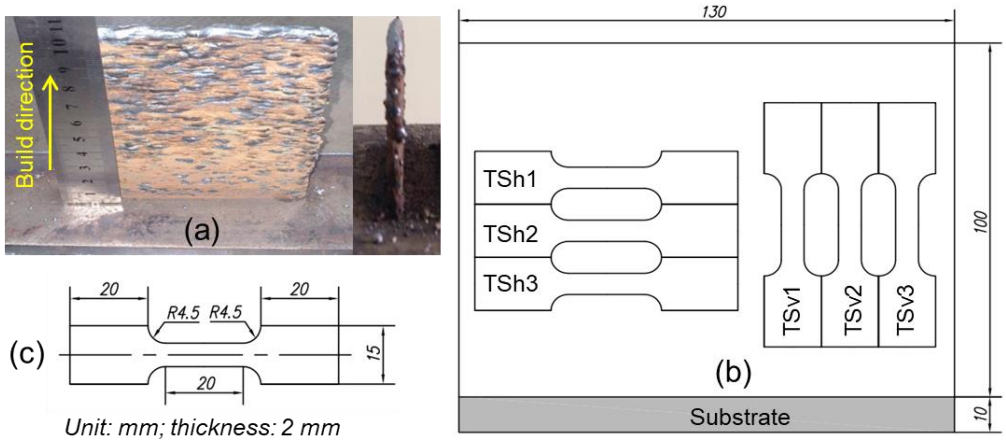

Figure 8. The built sample for the tensile testing (a), positions for cutting two groups of tensile specimens (b), and dimensions of tensile specimens (c).

As presented in Sections 3.1 and 3.3, the parameters used to build sample 2 (Table 2) allow the thin wall to be built with the most stable shape and the highest average hardness value in each region. Hence, these parameters were used to build a thin-walled sample on another substrate for the tensile tests. The same strategy and conditions presented in Section 2.2 were also applied for building this sample. Its dimensions are about 100 mm in height and 130 mm in length (Figure 8a).

To prepare the tensile test specimens, two side surfaces of the built thin wall were firstly machined to obtain an effective wall width of welded materials. Thereafter, two groups of tensile specimens in the horizontal and vertical directions (TSh*i* and TSv*i*, with *i* = 1, 2 and 3, Figure 8b) were cut by using a wire-cut electrical discharge machining (EDM) machine. Each group consists of three specimens. Their dimensions are presented in Figure 8c. The cross-section and length for examining tensile properties are 6 mm x 2 mm and 20 mm, respectively. The tensile tests were conducted on the tensile test machine (INSTRON 3369) of INSTRON Company with a cross head displacement speed of 1.2 mm/min and at room temperature.

Figure 9 presents the stress-strain curves of two tensile specimens TSv1 and TSh1, which are respectively representative for all specimens in two groups. It is found that the yield strength (YS) and ultimate tensile strength (UTS) of the horizontal specimens, which are perpendicular to the build direction (TSh*i*), are lower than those of the vertical specimens (TSv*i*). The average values of YS and UTS of specimens TSv*i* are 362 ± 8 (MPa) and 479 ± 7 (MPa), respectively, whereas the average values of YS and UTS of specimens TSh*i* are 320 ± 6 (MPa) and 429 ± 8 (MPa). This difference of YS and UTS values between two directions (parallel and perpendicular to the build direction) is due to non-uniform microstructures of the GMAW-based AM-built sample. In comparison to wrought A36 low-carbon steel (YS = 250 MPa and UTS = 400 – 550 MPa), the values of YS of all tensile specimens are higher, while their UTS values fall in the range of UTS values of wrought A36 low-carbon steel.

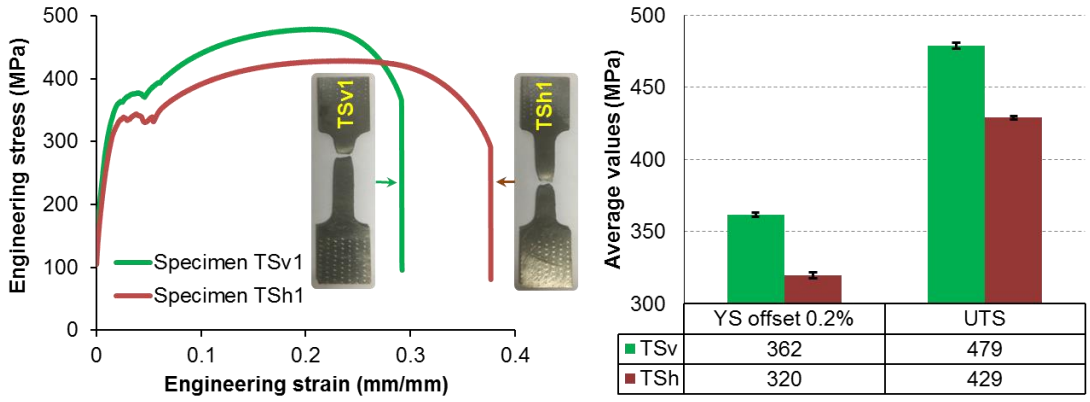

Figure 9. Stress-strain curves and average values of YS and UTS of specimens parallel (TSv*i*) and perpendicular (TSh*i*) to the build direction of the built thin-walled part.

4. CONCLUSIONS

This paper investigated the influence of the welding current on the shape and the microstructure of thin-walled low-carbon steel parts manufactured by the GMAW-based AM process. The welding current significantly influences on the shape of built thin-walled samples.

On the other hand, the welding current does not cause significant difference in terms of the microstructure type in each region of the wall. The microstructure of the wall consists of lamellar structures in the upper region, granular structures of ferrites with small amount of pearlites at grain boundaries in the middle region, and equiaxed grains of ferrites in the lower region. In terms of grain size, the increase in the welding current leads to coarser grains in microstructures of the built sample, and resulting in decreasing the hardness value. There is also a difference of tensile properties between the vertical and horizontal directions. The mechanical properties of GMAW-based AM-built parts are also comparable to those of wrought A36 low-carbon steel, which has similar chemical compositions in comparison with ER70S-6. The results obtained in this study give us a comprehensive understanding about the effects of the welding current in the GMAW-based AM process on the shape and the material properties of the low-carbon steel walls, and allow us to choose a suitable level of welding current for additive manufacturing thin-walled components.

Acknowledgements. This research is funded by Vietnam National Foundation for Science and Technology Development (NAFOSTED) under grant number 107.99-2019.18.

REFERENCES

1. Gibson I., Rosen D. W., Stucker B. - Additive Manufacturing Technologies, Boston, MA, Springer US, 2010.
2. Williams S. W., Martina F., Addison A. C., Ding J., Pardal G., Colegrove P. - Wire + Arc Additive Manufacturing, Mater. Sci. Technol. **32** (2016) 641-7.
3. Le V. T. - A preliminary study on gas metal arc welding-based additive manufacturing of metal parts, Sci. Technol. Dev. J. **23** (2020) 422-429.
4. Wu B., Pan Z., Ding D., Cuiuri D., Li H., Xu J., Norrish J. - A review of the wire arc additive manufacturing of metals: properties, defects and quality improvement, J. Manuf. Process. **35** (2018) 127-39.
5. Derekar K. S. - A review of wire arc additive manufacturing and advances in wire arc additive manufacturing of aluminium, Mater. Sci. Technol. **34** (2018) 895-916.
6. Zhang Z., Sun C., Xu X., Liu L. - Surface quality and forming characteristics of thin-wall aluminium alloy parts manufactured by laser assisted MIG arc additive manufacturing, Int. J. Light. Mater. Manuf. **1** (2018) 89-95.
7. Xiong J., Li Y., Li R., Yin Z. - Influences of process parameters on surface roughness of multi-layer single-pass thin-walled parts in GMAW-based additive manufacturing, J. Mater. Process. Technol. **252** (2018) 128-36.
8. Xiong J., Zhang G. - Adaptive control of deposited height in GMAW-based layer additive manufacturing, J. Mater. Process. Technol. **214** (2014) 962-8.
9. Suryakumar S., Karunakaran K., Chandrasekhar U., Somashekara M. - A study of the mechanical properties of objects built through weld-deposition, Proc. Inst. Mech. Eng. Part B J. Eng. Manuf. **227** (2013) 1138-47.
10. Liberini M., Astarita A., Campatelli G., Scippa A., Montevecchi F., Venturini G., et al. - Selection of Optimal Process Parameters for Wire Arc Additive Manufacturing, Procedia CIRP **62** (2017) 470-474.
11. Chen X., Li J., Cheng X., He B., Wang H., Huang Z. - Microstructure and mechanical properties of the austenitic stainless steel 316L fabricated by gas metal arc additive

manufacturing, Mater. Sci. Eng. A **703** (2017) 567-77.

12. Nguyen T. M., Nguyen V. H., Kim J. C. - The Microstructural Revolution of Ti-6Al-4V Specimens Fabricated by Selective Laser Sintering of Pre-alloyed Powders, Vietnam J. Sci. Technol. **57** (3A) (2019) 103-111.
13. Le V. T., Mai D. S. - Microstructural and mechanical characteristics of 308L stainless steel manufactured by gas metal arc welding-based additive manufacturing, Mater. Lett. **271** (2020) 127791.
14. Quintino L., Liskevich O., Vilarinho L., Scotti A. Heat input in full penetration welds in gas metal arc welding (GMAW), Int. J. Adv. Manuf. Technol. **68** (2013) 2833-2840.
15. Yang D., Wang G., Zhang G. - Thermal analysis for single-pass multi-layer GMAW based additive manufacturing using infrared thermography, J. Mater. Process. Technol. **244** (2017) 215-224.
16. Wu Q., Ma Z., Chen G., Liu C., Ma D., Ma S. Obtaining fine microstructure and unsupported overhangs by low heat input pulse arc additive manufacturing, J. Manuf. Process. **27** (2017) 198-206.
17. Haden C. V., Zeng G., Carter F. M., Ruhl C., Krick B. A., Harlow D. G. - Wire and arc additive manufactured steel: Tensile and wear properties, Addit. Manuf. **16** (2017) 115-123.